arXiv:1402.4931v1 [cond-mat.str-el] 20 Feb 2014

Phase diagram of the 1/3-filled extended Hubbard model on the Kagome lattice

Karim Ferhat and Arnaud Ralko
Institut Néel, UPR2940, Université Grenoble Alpes et CNRS, Grenoble, FR-38042 France
(Dated: February 21, 2014)

We study the phase diagram of the extended Hubbard model on the kagome lattice at 1/3 filling. By combining a configuration interaction approach to an unrestricted Hartree-Fock, we construct an effective hamiltonian which takes the correlations back on top of the mean-field solution. We obtain a rich phase diagram with, in particular, the presence of two original phases. The first one consists of polarized droplets of metal standing on the hexagons of the lattice, and an enlarged kagome charge order, inversely polarized, on the remaining sites. The second, obeying a local *ice-rule* type constraint on the triangles of the kagome lattice, is driven by an antiferromagnetically coupling of spins and is constituted of disconnected 6-spin singlet rings. The nature and stability of these phases at large interactions is studied via variational wave functions and perturbation theory.

I. INTRODUCTION

Lattice systems with geometrical frustration are at the center of intense theoretical and experimental research activity of nowadays condensed matter, thanks to the extremely rich exotic phases encountered. One of the most important features of frustrated systems is the presence, in the classical limit, of highly degenerate ground states. These states, under the presence of quantum fluctuations, yield unconventional phases generic either in fermionic and bosonic systems such as spin liquids[1,2], valence bond physics[3,4], pinball phases[5,6], fractionalized defects[7], and even supersolids[8,9]. Hence, frustration is at the crossroads of many disciplines, ranging from quantum antiferromagnets to optical lattices, via itinerant electrons and bosonic systems.

Intensively studied in quantum magnetism and in the study of spin liquid ground states, the role of frustration is more and more considered in fermionic systems[5–7,10,11]. Among the typical two dimensional lattices possessing a geometrical frustration, one can mention the triangular, checkerboard[8,12], Cairo-pentagonal[13,14], and kagome[10,15–19]. The latter is the most frustrated two dimensional lattice and, as a function of the electron filling, possesses several induced local constraint phases. At half filling, under strong Hubbard repulsion, the effective spin 1/2 model is expected to have a spin liquid ground state at very low temperature with a small or non-existing gap[20,21] while a more exotic scenario for a large unit cell valence bond crystal has been recently proposed[22,23]. The intense activity on this geometry is mainly due to the recent discovery of experimental compounds expected to be the ideal realization of such spin 1/2 quantum antiferromagnets, the Herbertsmithite[24–26]. More recently, at 1/2 or 2/3 filling fraction, anomalous quantum Hall effects of light under the presence of magnetic flux[27] and chiral spin liquid[28] and anyons[29] have been reported.

However, at lower filling, *i.e.* 1/3, only few works have been done so far. Let us cite studies on interaction induced topological phases[10], Mott-insulator transitions for spinless fermions[30] or fractionalization of defects with an extra bow-tie term[7]. The $1/3$ filling takes a special role in this system since the Fermi sea is at the *Dirac cones* at the corner of the Brillouin zone (K point) and the ground state is a semi-metal (SM). Under the presence of the Hubbard interaction, spin-charge density waves with antiferromagnetic spin stripes are stabilized[10], but this phase was enforced to preserve the translations. With nearest-neighbor interaction, a local constraint emerges, often called *ice-rule*, very reminiscent to those observed in spin-ices. Thus, the ground state manifold is macroscopically degenerate with a finite entropy at zero temperature. This has to be connected with the physics of hard-core bosons which arises in corner-sharing frustrating unit lattices such as the checkerboard[8,19], the pyrochlore or the Cairo-pentagonal lattices[13,14] for example. On such a manifold, the quantum fluctuations select a resonating plaquette phase by an order-to-disorder mechanism through a perturbation theory of the third order similar to that of RVB physics, and the local ice-rule constraint enforces the system to have exactly one doubly occupied site per triangle[7]. Despite the presence of all the ingredients –frustration, local constraint, ground state degeneracy, etc– needed to observe a very rich and exotic physics, the phase diagram of this model is still lacking in the literature, even at the mean-field level.

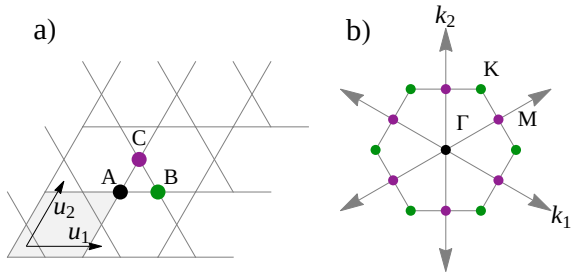

FIG. 1: (Color online). a) Example of a 3×3 kagome lattice with 3 sites per unit cell dubbed A, B and C. b) The Brillouin zone with $\mathbf{k}_1$ and $\mathbf{k}_2$ the reciprocal vectors of $\mathbf{u}_1$ and $\mathbf{u}_2$, the elementary translational vectors in real space defined in (a). The highest symmetry points Γ, M and K are depicted.

In this paper, we provide a theoretical study of the phase diagram of the extended Hubbard model at filling 1/3 at low and intermediate on-site and nearest neighbor interactions. In section II are presented the model and methods, as well as the physical quantities used to determine the phases. In particular, we briefly introduce the configuration interaction method (CI)[31–36] that we combine to an Unrestricted Hartree-Fock in order to partially bring back the correlations lost in the mean-

field decoupling. Section III gives an overview of the thermodynamic limit phase diagram and a brief description of the encountered phases, emphasizing two original ones, the droplet metal phase (DM) and a spin-charge density wave (SCDW). The identification of the phases, the extrapolation to the thermodynamic limit, and the stability of the phases upon the correlations by the CI are discussed in Section IV. Finally, the structure of the phases beyond the UHF and CI is discussed in Section V. We present a variational theory that helps in the understanding of the mechanism stabilizing the two peculiar phases, one being the presence of local polarized droplets of metal isolated by pins, and the other consisting of disconnected hexagons of 6 spin singlets.

II. MODEL AND METHODS

The model considered in this paper is the extended Hubbard model on the kagome lattice:

$$\mathcal{H} = -t \sum_{\langle i,j\rangle,\sigma} (c^\dagger_{i,\sigma} c_{j,\sigma} + h.c) + U \sum_i n_{i,\uparrow} n_{i,\downarrow} + V \sum_{\langle i,j\rangle} n_i n_j \quad (1)$$

where $c^\dagger_{i,\sigma}$ creates a fermion with spin σ at site i, $n_{i,\sigma} = c^\dagger_{i,\sigma} c_{i,\sigma}$ is the number of electrons with spin σ and $n_i = n_{i,\uparrow} + n_{i,\downarrow}$ the total density. U is the on-site Hubbard term, V the nearest neighbor Coulomb repulsion and $t > 0$ the hoping term. Throughout the paper, the lowest band is completely filled, corresponding to the 1/3 filling. As reported in the literature, at small interactions U and V, the system is a semi-metal (SM), while at large V (keeping U small) a resonating plaquette charge density wave (CDW) is stabilized[7,10,11,30,37,38]. Indeed, in this large V limit, the system is governed by a local constraint enforcing each triangle of the lattice[39] to have exactly only one doubly occupied site and the others empty. This ensures the ground state, at the electrostatic limit ($t = 0$), to be macroscopically degenerate. Then, a ring exchange of particles on a hexagon of order t^3/V^2 lifts this degeneracy and selects the CDW. How those two phases behave upon intermediate values of U is one of the questions addressed in this work.

The kagome lattice with periodic boundary conditions is defined by its linear size L, and has three sites per unit cell, called A, B and C in Fig.1. The number of sites is given by $N = 3L^2$. Most of the computations of the ground states performed in this paper have been done by using (i) an Unrestricted Hartree-Fock (UHF) and (ii) by partially bringing back on the top of this mean-field solution the correlations by using a Configuration Interaction on single and double excitations (SDCI) of the UHF Slater determinant[31–36]. This is achieved by the construction of an effective hamiltonian by projecting $\mathcal{H}$ onto this basis $\{\phi_i\}$ (detailed in the next section). As a reminder, in the standard UHF approach, the interaction terms $n_{i,\sigma} n_{j,\sigma'}$ are decoupled as a Hartree term $\langle n_{i,\sigma}\rangle n_{j,\sigma'} + n_{i,\sigma}\langle n_{j,\sigma'}\rangle - \langle n_{i,\sigma}\rangle\langle n_{j,\sigma'}\rangle$ and a Fock term $\langle c^\dagger_{i,\sigma} c_{j,\sigma'}\rangle c^\dagger_{j,\sigma'} c_{i,\sigma} + c^\dagger_{i,\sigma} c_{j,\sigma'}\langle c^\dagger_{j,\sigma'} c_{i,\sigma}\rangle - \langle c^\dagger_{i,\sigma} c_{j,\sigma'}\rangle\langle c^\dagger_{j,\sigma'} c_{i,\sigma}\rangle$. The sets $\langle n_{i,\sigma}\rangle$ and $\langle c^\dagger_{i,\sigma} c_{j,\sigma'}\rangle$, for i and $j \in [1, N]$, are computed self-consistently.

In order to characterize the phase diagram, we define a set of order parameters. The structure factor $M(\mathbf{q}) = \sqrt{\langle\psi_0|n(-\mathbf{q})n(\mathbf{q})|\psi_0\rangle/N}$, where $n(\mathbf{q}) = n_\uparrow(\mathbf{q}) + n_\downarrow(\mathbf{q})$ indicates spontaneous translational symmetry breaking of the ground state. Since at very large Coulomb repulsion V the system is governed by the local *ice-rule* constraints, we define the local triangle operators $\xi^\pm = \frac{6}{N}\sum_t w^0\rho^\pm_A + w^1\rho^\pm_B + w^2\rho^\pm_C$ with $\rho^\pm_i = n_{i\uparrow} \pm n_{i\downarrow}$ and $w = e^{i2\pi/3}$. $\xi^+ = 1$ for a phase obeying an ice-rule of 2 particles per triangle with exactly one doubly occupied site, and $\xi^- = 1$ if the ice-rule of the type two particles/one empty site is realized. Both order parameters are 0 in the homogeneous phase, and finite otherwise. To study the internal spin ordered phases, we define the operator $\rho^-_A\rho^-_B\rho^-_C$ which is finite if there are no vacant sites.

III. OVERVIEW OF THE PHASE DIAGRAM

The phase diagram of the 1/3-filled extended Hubbard model on the kagome lattice extrapolated to the thermodynamic limit from the UHF results up to $3 \times 36 \times 36$ site clusters is depicted in Fig.2. Four phases have been obtained in

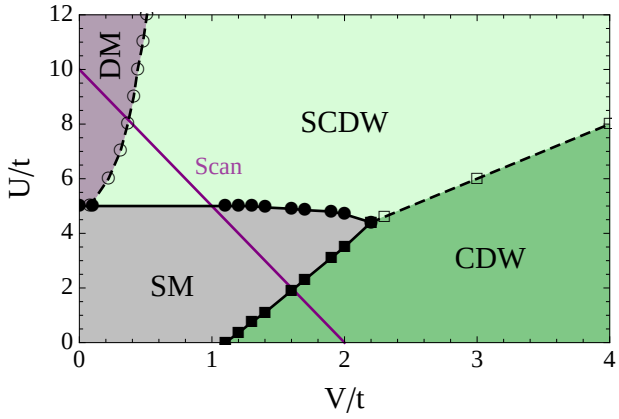

FIG. 2: (Color online). Phase diagram in the (V, U) plane. All points are extrapolations at the thermodynamic limit obtained by size scalings. The 4 phases are the semi-metal (SM), the resonating charge density wave (CDW), the spin-charge density wave (SCDW) and the droplet metal (DM). The line corresponds to the scan discussed in Fig.3.

the (V, U) plane, the semi-metal (SM), a charge density wave (CDW), a spin-charge density wave (SCDW) and a droplet metal (DM). As already mentioned, the first two phases have already been reported elsewhere[37–39]. For the CDW, a perturbative effective model of order t^3/V^2 maps the present model onto a quantum dimer model on the hexagonal lattice[11,37–39]. Indeed, in the classical limit $t = 0$ and $V \neq 0$, the ground state is macroscopically degenerate, and the configurations that minimize the energy obey a rule of *2 electrons per triangle with one doubly occupied site*. A finite t lifts this degeneracy and in the limit $t \ll V$ the system is effectively described by a hardcore dimer model on the honeycomb lattice[11,37,38] whose ground state consists of resonating plaquettes. The

mean-field treatment cannot capture the resonating plaquettes of the QDM, but its solution can be thought as its electrostatic counterpart[10]. This can be seen in the UHF local densities in Fig.4. A second order transition between the SM and the CDW is obtained. To the best of our knowledge, the two other phases reported in this work, namely the DM and SCDW phases, have not been reported so far[40]. Starting from the CDW phase in the large V regime, by increasing U with $U > 2V$, it is more favorable for the system to forbid double occupancies. This is happening through a first order phase transition. At the opposite of the recent paper of Wen *et al.*, since we do not restrict our phases to preserve translational symmetries, we obtain a $\sqrt{3} \times \sqrt{3}$ unit-cell phase with 6-spin antiferromagnetic hexagonal rings. All spin-*singlet* rings are disconnected by empty sites, as depicted in Fig.4-a (see the text for more details). We call this phase the spin-charge density wave (SCDW). Its phase transition with the SM is of second order. Eventually, at lower V interaction, the antiferromagnetic rings are not favored anymore, and the system prefers to separate up and down spins via another first order transition. One spin sector crystallizes on one third of the sites in order to form an enlarged kagome structure, the other sector forming disconnected half-filled hexagonal metallic rings on the remaining sites. This phase, called the droplet metal (DM), is stabilized thanks to the kinetic energy of those rings, as discussed in Section V. Except for the semi-metal, all the phases reported in this phase diagram break the translational symmetry, as a finite $M(K)$ indicates (see Fig.3). We provide in Section IV the complete analysis about the nature of these phases by UHF, then we describe the SDCI method and apply it to confirm their stability upon the correlations. We have followed the following strategy: First, we identify the phases by the UHF. Then, we check their stability deep in their domains and close to the phase boundaries by constructing a configuration interaction effective hamiltonian in the single and double excitations (SDCI) Slater basis (see next section for more details). We also verify that no new phases arise. Finally, in Section V, we have unraveled the mechanism of our phases by constructing a variational and perturbative theories based on our UFH and SDCI results at large U and V limit. This validates the present phase diagram.

IV. IDENTIFICATION OF THE PHASES AND THERMODYNAMIC LIMIT

A. UHF thermodynamic limit

In this section, we first present the thermodynamic limit phase diagram, displayed in Fig.2, extracted from finite size scalings of the UHF results. Then, we confirm the existence and the stability of all the phases beyond the mean-field level thanks to the single and double configuration interaction (SDCI). We have performed finite size scalings on the four order parameters, $M(\mathbf{q})$, $\xi^{\pm}$ and $\rho_A^- \rho_B^- \rho_C^-$ on clusters up to $3 \times 36 \times 36$ sites. To illustrate our results, we consider the scan line displayed in Fig.2, which passes through all the phases. The results are displayed in Fig.3. As one can see, size effects

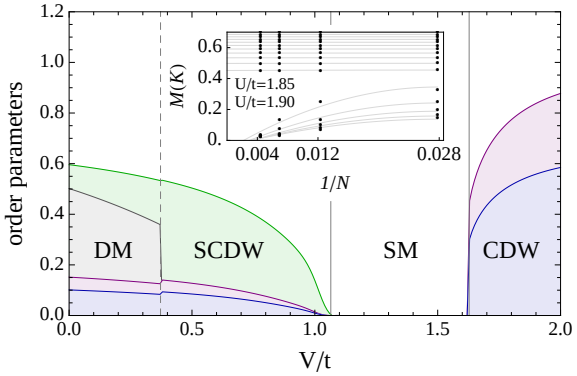

FIG. 3: (Color online). Behavior at the thermodynamic limit of the order parameters defined in the text along the scan line depicted in Fig.2 corresponding to $U = 10 - 5V$: (blue) $M(K)$, (gray) $\rho_A^- \rho_B^- \rho_C^-$, (green) ξ^- and (red) ξ^+. 4 distinct domains are observed, separated by continuous (second order) and dashed (first order) lines. Inset: size scaling of the CDW order parameter close to the transition with the SM; a clear change of behavior indicates the location of the phase transition.

are important (inset), as expected for the kagome lattice, but thanks to the large size clusters available, precise size scalings are performed. Our analysis reveals two second order phase transitions, between the CDW and the SM and between the SM and the CDW. The finite order parameter $M(K)$ (blue) at the TL indicates the spontaneous symmetry breaking of translations at the K point and thus a $\sqrt{3} \times \sqrt{3}$ unit-cell of 9 sites. The quantity $\rho_A^- \rho_B^- \rho_C^-$ (gray) is 0 as soon as on each triangle at least one zero magnetization site is present or finite otherwise. We observe that the DM phase is the only one with a finite TL value, all sites of each triangle are occupied. Finally, $\xi^{+(-)}$ (red, green) provide insights about the internal charge (magnetization) structure of each triangle. In Table I are reported which order parameter is compatible with which phase. All

Phases	$M(\mathbf{K})$	ξ^+	ξ^-	$\rho_A^- \rho_B^- \rho_C^-$
SM	0	0	0	0
CDW	✓	✓	0	0
DM	✓	✓	✓	✓
SCDW	✓	✓	✓	0

TABLE I: Classification of the possible phases that may occur in extended Hubbard model on the kagome lattice. Such phases can be distinguished from the density-density correlation $M(\mathbf{K})$, the internal triangular structures in charge (ξ^+) and magnetization (ξ^-), and the presence or not of a $s^z = 0$ site per triangle ($\rho_A^- \rho_B^- \rho_C^-$).

of them have been identified unambiguously within the UHF approach as seen in Fig.3. The corresponding density maps of the DM and the SCDW, either for the charge and the magnetization, are very close to the ones obtained by the SDCI (see below) depicted in Fig.4.

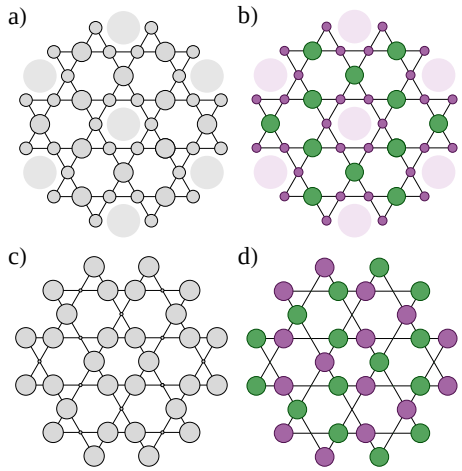

FIG. 4: (Color online). Snapshots of local charges (a,c) and spins (b,d) for the DM phase (a,b) at $U = 8$ and $V = 0$ and SCDW (c,d) at $U = 8$ and $V = 2$ obtained by SDCI on cluster of 108 sites. The larger the circle, the higher the density (charge and spin). The large disks illustrate the droplets of metal standing on the hexagons of the DM phase.

B. Configuration interaction: beyond the Hartree-Fock

In order to get further insights about the nature of the phases and their stability beyond the UHF, we have developed a *configuration interaction* method which aims to bring back the correlations on top of a mean-field single particle solution, here obtained by the UHF. The configuration interaction (CI) method[31–36], mentioned in Section II, consists in constructing an effective Hamiltonian $H_{ij}^{\rm eff}$ by projecting the microscopic Hamiltonian $\mathcal{H}$ in a subspace made of Slater determinants $\{\phi_i\}$, constructed in the single electron basis solution of a self-consistent unrestricted Hartree-Fock theory. If all Slater determinants are kept in the basis, then the full Hilbert space is spanned and $H_{ij}^{\rm eff}$ is nothing else but $\mathcal{H}$. This is usually referred to the full CI (FCI) in the literature[31]. Obviously, in this case, the limitations are the same that for the exact diagonalizations (ED), the Hilbert space is increasing exponentially and only small cluster sizes are available. An advantage to work with the Slater basis however, is that a simple energy criterion can be exploited. Indeed, at small and intermediate values of V and U, the correlations are expected to be well taken into account by single and double excitations from the Fermi sea. Hence, it is reasonable to truncate the basis to those processes and to restrict our effective Hamiltonian to this subspace. This is the so called single-double CI (SDCI). Note that this has been intensively studied in quantum chemistry where it has been shown that, for certain molecules, up to 80% of the correlation energy was restored. In Table II are reported the ground state energies obtained by ED (FCI), SDCI and UHF on a 2×2 cluster, the largest available by ED at the 1/3 filling. Keeping all single and double excitations above the Fermi sea corresponds to a total of 3489 Slater determinants. The parameters are chosen in the three non trivial phases, the CDW, the SCDW and the DM. For each of them, the SDCI clearly improves the GS energies, hence showing that correlations have been incorporated.

In our model, if the phases obtained by UHF are not stable under the correlations (for example the UHF is known to overestimate ferromagnetism), we expect the SDCI to stabilize other solutions. We were able to distinguish the four phases identified at the mean-field level. The snapshots of the local densities $n_{i,\sigma}$ of the DM and the SCDW phases are depicted in Fig.4. By turning on the correlations on top of the UHF solution, we found that all the phases are stable up to the largest cluster available by the CI, in our case the 6×6 unit cells (108 sites). Note that for such large cluster, the corresponding basis contains 263226945 determinants, which is not reachable by our computers. In order to reduce this size, it is possible to keep among the single and double excitations only those for which the excitation energy does not exceed a chosen cutoff $\Lambda_{\rm CI}$. By adjusting correctly this cutoff, one can find a compromise between the improvement of the GS wave function the size of the basis we want to deal with. For the $3\times6\times6$ site cluster, we have kept 1850220 Slater determinants for energy improvement of order of 10% on the GS energies. On the $3 \times 3 \times 3$ site cluster, for which no cutoff is required (97039 Slater determinants), the UHF energy is $14.4466(8)$ and $11.4323(0)$ for the SDCI in the SCDW phase at $U = 8$ and $V = 2$ (improvement of $20.97(5)\%$). In the DM phase at $U = 8$ and $V = 0$, the UHF gives $-24.9667(2)$ against $-28.7069(6)$ for the SDCI ($14.98(0)\%$). In Fig.4 are depicted the local charge and spin densities obtained by SDCI on the 108 site cluster, either for the DM and the SCDW phases. For information, in our computations, the change in the density values between the SDCI and the UHF never exceeded 3-4%, even close to the phase boundaries. This indicates that (i) these phases are stable upon the correlations, and (ii) the UHF phase diagram at the TL of Fig.2 captures the essential physics. Let us conclude this section by a remark concerning the phase boundaries of Fig.2. In this work, we have employed the SDCI to validate the presence of the main phases beyond the UHF and to verify whether or not new phases could be stabilized. Hence, we have focused deep in their domains, and made checking close to the main transitions. The question of the exact location of the boundaries within this approach requires an optimized methodology in selecting the active determinants, in order to reduce the size of the basis while keeping the correlations strong[34–36]. This is left for another work.

Phases	(U, V)	UHF	SDCI	ED (FCI)
DM	$(8, 0)$	$-10.818(4)$	$-12.801(5)$	$-14.071(9)$
SCDW	$(8, 2)$	$6.819(1)$	$5.199(0)$	$4.032(1)$
CDW	$(0, 2)$	$-5.820(9)$	$-5.985(6)$	$-6.430(1)$

TABLE II: Ground state energies of the different phases obtained by the three methods used in this work, here on a 2×2 cluster (12 sites) for various parameter sets.

V. VARIATIONAL APPROACH AT LARGE U AND V

Let us now try to understand the characteristics of the DM and the SCDW phases by considering the large U and V limit.

At large $U \gg V$, we find a phase which is the separation between *pins* (one electron) on each site of an enlarged kagome lattice and *balls* of 3 polarized electrons on each hexagon, that we expect to be in a metallic state. As a first approximation, one could think that these hexagons are isolated by the pins, as suggested by the real space density maps of the DM depicted in Fig.4-(c,f). To validate this picture, we have calculated the energy of the variational wavefunction (VWF) $|\psi\rangle = [\bigotimes_i |i\rangle] \otimes [\bigotimes_h |\hexagon_h\rangle]$ where the first product is over the sites of the enlarged kagome lattice and the second over all its hexagons. $|\hexagon_h\rangle$ is the ground state of an extended Hubbard model of 3 spinless electrons on a ring:

$$H_{\hexagon} = -t \sum_{i \in \hexagon} \left[(c_i^\dagger c_{i+1} + h.c) + V n_i n_{i+1} \right]. \qquad (2)$$

By computing the ground state energy and the kinetic operator $\hat{P} = (c_0^+ c_1 c_2^+ c_3 c_4^+ c_5 + h.c.)$ (the sites are labelled clockwise from 0 to 5), an inflexion point appears about $V \simeq 3t$. For $V < 3t$, the ground state is metallic. At $V = 0$, the ground state on each hexagon is a simple metal of three electrons, and in terms of local momenta k on the 6-site ring, the wavefunction is trivially given by the product state of the single electron Bloch states $|\hexagon_h\rangle = |k^0\rangle \otimes |k^+\rangle \otimes |k^-\rangle$, where $k^0 = 0$, and $k^\pm = \pm\pi/3$, with energies $E_0 = -2t$, $E_\pm = -t$ respectively. By applying the perturbation theory on $|\psi\rangle$ at large U, we find a correction to the energy as $E_{k^0} = -2t - 4\frac{t^2}{U}$, $E_{k^\pm} = -t - 3\frac{t^2}{U}$, and for the pins $E_i = -10\frac{t^2}{U}$, for a total variational energy $E_{\rm VWF} = -4t - 34\frac{t^2}{U}$. In Fig.5 is depicted the GS energies at $V = 0$ obtained by UHF and the variational energy obtained from the VWF with metallic hexagons; their agreement is excellent.

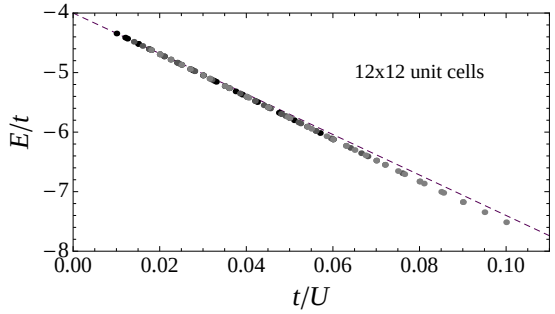

FIG. 5: (Color online). Agreement between the UHF energy and the variational wave function based on metallic hexagons for the DM phase. We show several scans from $t = 0.5$ (darker points) to $t = 1$ (lighter points). Each scan is made from $U = 10$ to $U = 50$. The dashed line is the energy expected in the DM phase $E = -4t - 34\frac{t^2}{U}$.

We turn now on the SCDW. In the large U limit, at $t = 0$, there are no double occupancies and the system, for any finite V, enters an *ice-rule* constraint of 2 electrons per triangle. Its ground state manifold is macroscopically degenerate and consists of closed loops of various lengths. When the quantum fluctuations t are turned on, the UHF and the SDCI select the smallest possible loops as observed in Fig.4-d. From a perturbation theory, there are two types of processes which can lift this degeneracy: an antiferromagnetically coupling of spins of order $\sim t^2/(U - V)$ at the second order, and resonating plaquette terms (ring exchange of 3 electrons on a hexagon) in $\sim t^3/V^2$ at the third order, similar to those of the QDM[37] at $U = 0$ and $V \gg t$. Unfortunately, neither the UHF (mean-field) neither the SDCI (up to double excitations) allow to distinguish which process is dominant in function of U and V. All we can say is that, at large enough V and $U \gg V$, the Heisenberg mechanism will be obviously favored. But let us go back to Eq. (2) and $|\psi\rangle$. The inflexion point in $\langle \hat{P} \rangle$ appearing around $V \simeq 3$ indicates that $\sim t^3/V^2$ ring exchange terms become dominant for higher V and thus the DM is destroyed at such large values of V. At the mean-field level, the UHF snapshot would be similar to that of Fig.4-d, but now the resonating hexagons are no longer the same than the heisenberg loop-6 discussed above. Hence, two scenarios are possible at the transition of the DM; (i) the system enters a phase with resonating plaquettes separated by pins based on our variational approach, then a further transition to a spin state driven by Heisenberg couplings is stabilized (with no pins); (ii) the Heisenberg state is selected right away. Our UHF and SDCI results present a phase transition about $V \simeq 0.25$ up to $U = 12t$, which is much smaller than $V \simeq 3$ at which the internal structure of the hexagon is changing. This seems to indicate that scenario (ii) is favored. Or in this case, based on the results of Fig.4-d, a ground state made of 6-spin singlet hexagons of energy per site $E_6 \simeq -0.467(1)$ is selected among the degenerate configurations. This is what we call the spin-charge density wave (SCDW). Finally, let us compare our results with previous work. In Wen *et al.* paper[10], since no translational symmetry breaking is allowed, a stripe phase with disconnected antiferromagnetic chains are obtained. In their case, the quantum fluctuations of the perturbation theory lowers the classical energy by $E_c = \frac{1}{4} - \log 2 \simeq -0.443(1)$. The hexagonal spin chain is then more likely when the symmetry constraint is removed, as confirmed by the snapshots of the SCDW depicted in Fig.4-(c,d).

VI. CONCLUDING REMARKS

In this paper, we have studied an extended Hubbard model of spinful electrons on the kagome lattice at 1/3 filling. In addition to two already known phases, the semi-metal (SM) and the charge density wave (CDW), we have established the presence of two original phases, the droplet metal (DM) and the spin-charge density wave (SCDW) stabilized at intermediate U and V.

We have first used an unrestricted Hartree-Fock approach in order to extract the phase diagram at the TL. We have then constructed an effective configuration interaction hamiltonian by projecting the microscopic model onto a basis of Slater determinants containing the UHF wave function, and all single

and double excitations (SDCI). This allows for bringing back partial correlations on top of the UHF solution. For various sets of parameters, the ground state energy (and related GS) is strongly improved (up to 25%). We have confirmed that (i) no new phases are stabilized by the correlations and (ii) the two original phases, namely the DM and the SCDW, are very robust against the correlations.

Finally, to get more insights about the nature of two new phases, we have performed a variational approach as well as a perturbation theory. We have shown that the properties of the droplet metal (DM) is perfectly captured by the UHF and explained by our variational wave function. It consists of polarized pins (electrons) standing on the sites of an enlarged kagome lattice, separating droplets of metal living on the remaining hexagons. The second important phase, the spin-charge density wave (SCDW), is driven by Heisenberg interactions and leads to loop-6 ring isolated spin states. Note that we have discussed the possibility of a third phase that could arise in the system, close to the DM but with resonating plaquettes instead of metallic droplets on the remaining hexagons. In some sense, this would correspond to an internal crossover of the hexagon states, the pins remaining unchanged. However, within our approaches, this phase does not seem to be stabilized at the intermediate parameters considered in this work. Instead, the DM and the 6-spin singlet SCDW are the more stable.

Note added. – We became aware, at the very end of this project, of related work by F. Pollmann *et. al* (Ref. [40]), where the authors have considered an effective model of Eq. (1) at large U and V limit. We thank F. Pollmann for stimulating discussions about their results corroborating the existence of the phases reported in this manuscript.

Acknowledgements – A.R. is grateful to F. Mila for insightful remarks about the stability of the phases. We thank S. Fratini for enlightening discussions and his careful rereading of the manuscript. A.R. thanks G. Bouzerar and M.-B. Lepetit for their valuable comments about the methods used in this paper. This work is supported by the French National Research Agency through Grants No. ANR-2010-BLANC-0406-0 NQPTP and No. ANR-12-JS04-0003-01 SUBRISSYME.

[1] G. Misguich, D. Serban, and V. Pasquier, Phys. Rev. Lett. **89**, 137202 (2002).
[2] M. Hermele, Y. Ran, P. A. Lee, and X.-G. Wen, Phys. Rev. B **77**, 224413 (2008).
[3] D.S. Rokhsar and S.A. Kivelson, Phys. Rev. Lett. **61**, 2376 (1988).
[4] R. Moessner and S.L. Sondhi, Phys. Rev. B **63**, 224401 (2001).
[5] J. Merino, A. Ralko, and S. Fratini, Phys. Rev. Lett. **111**, 126403 (2013).
[6] F. Trousselet, A. Ralko, and A. M. Oleś, Phys. Rev. B **86**, 014432 (2012).
[7] A. Ruëgg, and G. A. Fiete, Phys. Rev. B **83**, 165118 (2011).
[8] A. Ralko, F. Trousselet and D. Poilblanc, Phys. Rev. Lett. **104**, 127203 (2010).
[9] F. Trousselet, P. Rudea-Fonseca, and A. Ralko, Phys. Rev. B **89**, 085104 (2014).
[10] J. Wen, A. Rüegg, C.-C J. Wang, and G. A. Fiete, Phys. Rev. B **82**, 075125 (2010).
[11] F. Pollmann, P. Fulde, and K. Shtengel, Phys. Rev. Lett. **100**, 136404 (2008).
[12] S. Wessel, Phys. Rev. B **86**, 140501(R) (2012).
[13] A. Ralko, Phys. Rev. B **84**, 184434 (2011).
[14] I. Rousochatzakis, A. M. Laüchli, and R. Moessner, Phys. Rev. B **85**, 104415 (2012).
[15] O. Cepas, and A. Ralko, Phys. Rev. B **84**, 020413(R) (2011).
[16] D. Poilblanc, and A. Ralko, Phys. Rev. B **82**, 174424 (2010).
[17] S. V. Isakov, S. Wessel, R. G. Melko, K. Sengupta, and Y. B. Kim Phys. Rev. Lett. **97**, 147202 (2006).
[18] T. Ohashi, N. Kawakami, and H. Tsunetsugu, Phys. Rev. Lett. **97**, 066401 (2006).
[19] M. Indergrand, A. Läuchli, S. Capponi, and M. Sigrist, Phys. Rev. B **74**, 064429 (2006).
[20] O. F. Syljuasen and A.W. Sandvik, Phys. Rev. E **66**, 046701 (2002).
[21] K. Louis and C. Gros, Phys. Rev. B **70**, 100410 (2004).
[22] R. R. P. Singh and D. A. Huse, Phys. Rev. B **76**, 180407 (2007).
[23] G. Evenbly and G. Vidal, Phys. Rev. Lett. **104**, 187203 (2010).
[24] L. Santos et al., Phys. Rev. Lett. **93**, 030601 (2004).
[25] B. Damski et al., Phys. Rev. A **72**, 053612 (2005).
[26] T. Matsubara and H. Matsuda, Prog. Theor. Phys. **16**, 569 (1956).
[27] A-L. Gadsbolle, H. Francis Song, and K. Le Hur, Phys. Rev. A **86**, 053804 (2012).
[28] F. Wang and A. Vishwanath, Phys. Rev. B **74**, 174423 (2006).
[29] B. Bauer, L. Cincio, B. P. Keller, M. Dolfi, G. Vidal, S. Trebst, and A. W. W. Ludwig, cond-mat:1401.3017 (2014).
[30] S. Nishimoto, M. Nakamura, A. OBrien, and P. Fulde, Phys. Rev. Lett. **104**, 196401 (2010).
[31] *Relativistic and Electron Correlation Effects in Molecules and Solids*, Edited by G.L. Malli, Plenum Press, New York (1994).
[32] B. Friedman and G. Levine, Phys. Rev. B **55**, 9558 (1997).
[33] E. Louis, F. Guinea, M.P. López Sancho, and J.A. Vergés, Phys. Rev. B **59**, 14005 (1999).
[34] S. Li, J. Ma, and Y. Jiang, Int. Nat. J. Quant. Chem. **78** 153 (2000).
[35] C.F. Bunge and R. Carbó-Dorca, J. Chem. Phys. **125** 014108 (2006).
[36] M. Sambataro, D. Gambacurta, and L. Lo Monaco, Phys. Rev. B **83**, 045102 (2011).
[37] S. Nishimoto, M. Nakamura, A. O'Brien, and P. Fulde, Phys. Rev. Lett. **104**, 196401 (2010).
[38] A. O'Brien, F. Pollmann, and P. Fulde, Phys. Rev. B **81**, 235115 (2010).
[39] R. Moessner, S. L. Sondhi, and P. Chandra, Phys. Rev. B **64**, 144416 (2001).
[40] F. Pollmann, K. Roychowdhury, C. Hotta, and K. Penc, *unpublished* (2014).